



Article

Influence of the Oscillation Parameters Amplitude and Frequency on the Microstructure of Laser-Welded Thin Nitinol Foils

Danka Katrakova-Krüger ¹, Sabine Weichert ¹ and Christoph Hartl ^{2,*}

¹ Material Laboratory, Faculty of Computer Science and Engineering Science, Technische Hochschule Köln, Steinmüllerallee 1, 51643 Gummersbach, Germany; danka.katrakova-krueger@th-koeln.de (D.K.-K.); sabine.weichert@th-koeln.de (S.W.)

² Manufacturing Technology, Faculty of Automotive Systems and Production, Technische Hochschule Köln, Betzdorfer Str. 2, 50679 Cologne, Germany

* Correspondence: christoph.hartl@th-koeln.de; Tel.: +49-221-8275-2550

Abstract: Laser welding has become well established for joining Ni-Ti-based shape memory alloys and extends the manufacturability of highly functional components with complex geometries. Published studies on the effect of laser welding on alterations to microstructure and properties of these alloys, however, mainly deal with conventional component dimensions and linear laser beam movement. In view of the increasing importance of microtechnology, research into joining of thin-walled Ni-Ti components is therefore of interest. At the same time, studies comparing oscillating and linear beam movement on other materials and the authors' own work on Ni-Ti materials suggest that oscillating beam movement has a more favorable effect on alterations in material properties and microstructure. Therefore, laser welding of foils made of Ni55/Ti45 with 125 μm thickness was systematically analyzed using a fiber laser and circular oscillation. Amplitude A and frequency f were varied from 0 to 200 μm and 0 to 2000 Hz, respectively. Microstructural analysis showed that by increasing the frequency, grain refinement could be achieved up to a certain value of f . An increasing amplitude led to decreasing hardness values of the weld seam, while the influence of f was less pronounced. The analysis of the weld material using chip calorimetry (Flash DSC) revealed that the beam oscillation had fewer effects on the change in transformation points compared to a linear beam movement.

Keywords: laser welding; laser beam oscillation; Ni-Ti shape memory alloys; characterization

Academic Editor: Dulce Maria Rodrigues

Received: 22 December 2024
Revised: 17 January 2025
Accepted: 20 January 2025
Published: 23 January 2025

Citation: Katrakova-Krüger, D.; Weichert, S.; Hartl, C. Influence of the Oscillation Parameters Amplitude and Frequency on the Microstructure of Laser-Welded Thin Nitinol Foils. *J. Manuf. Mater. Process.* **2025**, *9*, 32. <https://doi.org/10.3390/jmmp9020032>

Copyright: © 2025 by the authors. Licensee MDPI, Basel, Switzerland. This article is an open access article distributed under the terms and conditions of the Creative Commons Attribution (CC BY) license (<https://creativecommons.org/licenses/by/4.0/>).

1. Introduction

Ni-Ti alloys are used as shape memory alloys (SMAs) in numerous important technical fields, such as aerospace, automotive engineering, microelectromechanical technology, civil infrastructure, and biomedical and medical technology [1–7]. They are considered to be one of the most frequently applied type of SMA, owing to the particular characteristics concerning shape memory effect, superelasticity, biocompatibility, and resistance to fatigue and corrosion [6–9]. The properties of SMAs concerning the shape memory effect and superelasticity are typically based on solid–solid-phase transformations between martensite and austenite phases that generally is initiated by temperature change or external loads [8–11].

However, manufacturing innovative products made of Ni-Ti alloys with a complex design and providing enhanced functionality through material properties such as shape memory and superelasticity is difficult using conventional production processes. Techniques such as casting, forming, and machining encounter problems due to the material's difficult workability [12–16], although newer developments in additive manufacturing are showing promising results, e.g., [17,18]. The assembly of basic structures using welding to generate more complex geometries offers a possible alternative to these processes. When fusion welding processes are used to join Ni-Ti alloys, however, functional and mechanical properties in the joined areas are significantly impacted as a result of thermally induced mechanisms and the formation of chemical impurities [5]. Laser welding has therefore emerged as one of the most widely studied and applied group of fusion welding processes for Ni-Ti alloys, as it is associated with minimal thermal effects [9]. Compared to other fusion welding processes, it offers the advantages of low heat input, high energy density, narrow heat-affected zone (HAZ) and high reproducibility [5,7,9,12]. Nevertheless, the laser-welding process can influence the transformation temperatures from martensite to austenite on heating, A_s (start of austenite transformation) and A_f (finalization of transformation), and on cooling from austenite back to martensite, with the starting temperature M_s and the temperature M_f on completion of the transformation, to a more or less pronounced degree depending on the parent material's initial conditions [19]. Likewise, for Ni-Ti alloys the absorption of oxygen during the welding process influences the transformation temperatures and causes a decrease in comparison to the parent material by fostering Ti-rich secondary phases [9,20]. It seems that the shape memory properties are less impacted by the laser-welding process, which is important, for example, for the use of the produced Ni-Ti workpieces for actuators, whereby the degree of recovery of the initial geometry depends on the amount of strain applied [9]. Regarding the superelastic properties after joining, which depend on various laser and welding parameters, it must be expected that these are less pronounced compared to the parent material [9].

Overall, the laser welding of Ni-Ti alloys has already been studied intensively and summarized in detail in various review articles and books, e.g., [6,7,9,12]. Oliveira et al. [9] provided a very detailed discussion of the state of scientific work on the joining of Ni-Ti alloys by fusion welding and solid-state methods, considering also joining of Ni-Ti with other materials. He pointed out that main challenges in welding Ni-Ti consist of decrease in strength values, generation of intermetallic compounds, alterations in phase transformations and transformation temperatures, and modifications to the shape memory effect and superelastic behavior. It was stated in [9] that the use of laser welding has been most frequently investigated and used due to its lower thermal influence. The review article by Mehrpouya et al. [6] was specifically devoted to the laser welding of Ni-Ti alloys and discussed scientific papers that were dealing with the change in strength values, cyclic deformation behavior, hardness, corrosion behavior and microstructure, and metallurgical effects. In particular, the authors also summarized publications on post-weld heat treatment processes and how these can be applied to mitigate the adverse effects of the alterations of properties caused by the welding process [6]. In [12], Metha et al. provided an overview of the processing of SMAs in book form and discussed in this context different joining technologies. Regarding the topic of laser welding of SMAs, Nd:YAG and fiber lasers were described as the preferred beam sources, influences of the process parameters on the welding result were discussed, and typical forms of the microstructure of welded Ni-Ti alloys were illustrated [12]. Parimanik et al. [7] demonstrated the scientific advances in laser welding of Ni-Ti alloys on the basis of a systematic literature analysis, with a focus on investigations into mechanical, metallurgical, and corrosion-relevant changes caused by the welding process. In particular, only a small proportion of published literature was

found that dealt with optimization of process parameters, which offers scope for more research [7].

However, there are only a few published works on the laser welding of very thin Ni-Ti foils in the sub-millimeter range, which is the focus of the present study. For example, these semi-finished products are of relevance for reconfigurable mobile phone antennas and temperature-sensitive actuators [21,22]. It has been summarized in [6] that, for laser welding of thin foils, Nd:YAG and fiber lasers offer benefits over CO₂ lasers with regard to a reduced heat-affected zone and greater energy absorption as a result of the shorter wavelength, and that pulsed lasers are preferred. Khan et al. [23] applied a pulsed Nd:YAG laser for the welding of foils made of a Ni-Ti alloy with 55.8 wt.% Ni with a thickness of 370 μm and studied alterations of mechanical and pseudoelastic characteristics, which were decisively influenced by the welding parameters. Chan et al. [24] welded 250 μm thick foils produced from an SMA with 55.91 wt.% Ti employing a 100 W CW fiber laser. Cellular dendrites dominated the welds with minor fractions of intermetallic Ni₃Ti phases, and *A_s* and *M_s* were reduced [24]. Gong et al. [25] presented results on the welding of foils with 200 μm thickness applying a Nd:YAG laser and found almost identical transformation behavior of the welded samples after annealing as in the annealed starting material. Quintino et al. [26] examined the joining of cold-rolled foils and sheets of 340 and 1000 μm thickness made of an SMA with 50.8 at.% Ni applying a pulsed Nd:Yag laser and described the characterization of the microstructure in the fusion zone (FZ) and HAZ. Oliveira et al. [27] studied the occurrence of martensite after Nd:YAG laser welding in 1000 μm thick sheets of an austenitic SMA with 50.8 at.% of Ni. HAZ and FZ showed martensite fractions and the appearance of precipitations (Ni₄Ti₃) in the HAZ was discussed [27]. Kannan et al. [28] used a Yb:YAG laser to weld sheets made of a Ni-Ti alloy with 1000 μm thickness and applied optimization methods to determine optimal welding parameters in terms of penetration depth, weld width, hardness, and corrosion resistance. Datta et al. [29] employed a fiber laser with 2000 W and investigated joining of 1000 μm thick sheets containing 52 at.% Ni. The weld seams exhibited intermetallic phases, e.g., Ni₃Ti and Ti₂Ni, which were considered responsible for the decrease in strength and elongation at fracture, together with microstructural alterations caused by the joining process [29].

It should be noted that these works reported partially different levels of success in the optimization of welding parameters and joint properties. Nevertheless, they indicate that there is still room for improvement in the welding of thin-walled Ni-Ti structures with regard to improved microstructure, the preservation of functional properties and mechanical characteristics. One approach to achieving improved welding results for this particular application is seen in the use of an oscillating laser beam movement during the welding process [30]. This strategy, which so far has not been systematically analyzed for welding of Ni-Ti alloys with lasers, has already been applied to the laser welding of a number of other materials and has shown advances in welding results [31,32] in terms of improvements in gap tolerance [33,34], limiting spatter [35,36], grain size reduction [35,37–41], porosity defect suppression [37,38,42–44], homogenization of alloying elements [31,32,45], influencing formation of solidification cracks [31,35], and mechanical properties [33,35,37,39,40,42,46,47].

Laser beam oscillation broadens the laser energy distribution along the weld with a reduction in mechanical stresses and improved possibilities for the migration of solutes [31]. Temperature gradients and solidification rates can be influenced by oscillation [31]. By the broadening of the weld, the energy density introduced is reduced, which limits the growth of cellular and dendritic grains [31]. Furthermore, the oscillating laser beam motion creates a stirring effect [31,45,46] that alters the flow and solidification behavior in the molten pool, causing, for example, the fragmentation of gas inclusions and, with this, a

reduction in porosity [43], initiating dendrites to break, and supporting the movement of the solute, whereby its complete diffusion can considerably decrease solidification crack susceptibility [31].

Specific parameters of the oscillation that can be applied to influence the welding result are frequency f , amplitude A , and shape of the oscillation [46]. For example, Zhao et al. [46] found with experimental and theoretical investigations into the laser welding of an Invar alloy with circular oscillation that the introduction of a low oscillation frequency of 50 Hz was beneficial to promoting grain refining, but that this effect was not obvious when increasing f above 100 Hz due to heat accumulation. With regard to improvements in tensile strength and elongation at fracture, an increase of 5.8 and 23.7%, respectively, was observed for the welds with $f = 50$ Hz compared to samples welded without oscillation [46]. Cai et al. [47] conducted experimental and theoretical work to investigate f and A for the laser welding of an aluminum alloy with circular beam movement and found that the energy density at the sides of the heat input was higher than in the center and that the ratio of depth to width of the weld decreased by about 24 and 59%, respectively, when f was increased from 100 to 300 Hz and A from 1 to 3 mm. A significant reduction in porosity was observed for $f > 200$ Hz at $A = 2$ mm and for $A > 2$ mm at $f = 200$ Hz [47]. In these investigations, the use of oscillation resulted in an increase in hardness of the FZ by 3.7%, which was attributed to grain refinement and more uniformly distributed phases, and an increase in tensile strength and elongation at fracture by 65.1 and 30.6%, respectively, which was ascribed to the larger bearing surface and the lower stress concentration [47]. Using a numerical multi-physics-based model, Ke et al. [38] examined the laser welding of an aluminum alloy for the circular and infit oscillation patterns with regard to the influence on the resulting porosity. Also, here, the results showed that the porosity was reduced with the application of the oscillation and could be inhibited at a frequency of 200 Hz. Dong et al. [48] investigated experimentally and theoretically the influence of f and A for different oscillation patterns (linear, circular, 8-shaped, and so-called infinity oscillations) on the formation of the weld for stainless steel. They found, among others, that, for a constant heat input, an increase in f between 10 and 50 Hz resulted in a decrease in weld width and that small values of f or large values of A led to a weaker flow in the weld area and vice versa [48]. Zhou et al. [39] examined various oscillation patterns (linear, 8-shaped, and infinity oscillations) for the laser welding of an aluminum alloy in terms of the formation of the weld seam, the microstructure, and the mechanical characteristics, both experimentally and theoretically. In these investigations, the results indicated that the application of the oscillation patterns improves the weld morphology, refines grains, and increases the hardness and strength of the weld, and it was shown that the 8-shaped oscillation pattern led to the highest tensile strength, about 63.8% higher than the one of welding without oscillation [39]. In addition to the opportunities mentioned above of improving tensile strength, elongation and hardness values of welded joints by means of oscillation, Hensel et al. [33] demonstrated improvements in the fatigue strength of laser welded joints of case-hardening steel when laser beam oscillation was used to bridge gaps between the components to be joined compared to welding without oscillation and with a focused beam.

On the basis of design of experiments (DoE) methods and a certain number of specifically selected experiments, it was possible to demonstrate in a first study on the welding of 125 μm thick Ni-Ti foils that an application of laser beam oscillation also resulted in advantages concerning improved mechanical properties and weld seam microstructure for this alloy. [30]. The aim of this study was to identify optimal welding parameters for high joint strength, which was successfully achieved [30]. However, since these investigations have only considered selected parameter settings, a number of research questions remained unanswered. These include the issue of how exactly amplitude and frequency

affect the formation of the weld, hardness profile, grain size distribution of the microstructure, and, in particular, the extent to which alterations in transformation behavior can be influenced by varying A and f . Knowledge of these relationships, which have not yet been analyzed for either SMAs or for the Ni-Ti alloy under consideration here, enables parameter settings to be selected that allow the properties of the weld to be better adapted to a respective application. The present article is focused on clarifying these topics and presents the findings of systematic research on the influences of amplitude and frequency on the formation of the weld seam, the microstructure and hardness values, and on alterations in the transformation temperatures.

2. Materials and Methods

For the fabrication of the specimens for the welding investigations, annealed foils made of a Ni-Ti alloy with 55 wt.% Ni and 45 wt.% Ti were used. The individual specimens with 125 μm thickness were cut out of the foils as strips with a width of 9.5 mm, cleaned and degreased. The welds were performed in a bead-on-plate configuration under a shielding gas bath using argon (Figure 1a) employing an YLR-50-SM ytterbium CW fiber laser (IPG Laser, Burbach, Germany) with a maximum power of 50 W. The wavelength of the laser beam was 1070 nm, and the focal spot diameter was 32 μm . A Shemo STT-2238 galvanometer scanner (SK Latronics Laser, Aachen, Germany) equipped with f-Theta lens and controllable deflection mirrors was used to realize the laser beam movement, and a circular oscillation pattern was selected (Figure 1b).

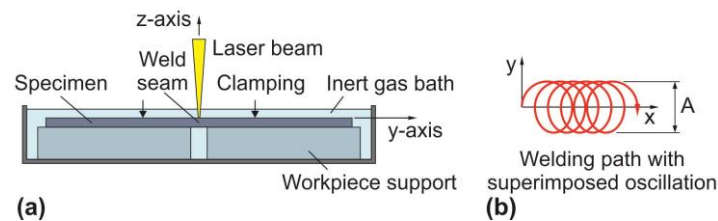


Figure 1. Representation of laser-welding experiments (schematic): (a) experimental set-up; (b) superimposed oscillation. Source: adapted from [30].

The values listed in Table 1 were selected as parameters for the welding process for the laser power P , the welding speed v , the frequencies f , and amplitudes A . Welds without oscillation were also carried out for the purpose of comparison, using the values given in Table 1. P and v were determined in the previously mentioned work [30] for the samples used here as part of a DoE study. These values resulted in the highest mean tensile strengths σ_{UTS} for the welded samples, both with linear welding (LW) ($\sigma_{\text{UTS}} = 225$ MPa) and with oscillation (OW) with $f = 300$ Hz and $A = 100$ μm ($\sigma_{\text{UTS}} = 236$ MPa) [30].

Table 1. Laser-welding parameters.

Configuration	P (W)	v (mm/s)	f (Hz)	A (μm)
Oscillating welding (OW)	40	24	100 300 600 1200 2000	100 400 800
Linear welding (LW)	40	24	0	0

To analyze the welding results, images of the upper and lower sides of the weld were first taken using a digital Keyence VHX 7000N microscope (Keyence Deutschland, Neu-Isenburg, Germany). The samples were then divided, cold mounted in an epoxy resin filled with nickel powder, ground, and polished with an SiO_2 -based polishing suspension with a grain size of 0.05 μm . A scanning electron microscope (SEM), type Hitachi SU 5000 (Hitachi High-Technologies Europe, Krefeld, Germany), was used to observe the

microstructure and to subject the samples to electron backscatter diffraction (EBSD) analyses and energy-dispersive X-ray spectroscopy (EDX). The evaluation of these analyses was supported by the software package Aztec 5.0 SP1 (Oxford Instruments, Oxon, UK). Microhardness measurements were performed by applying the DIN EN ISO 6507-1 standard [49] using a Qness Q10A+ system (ATM Qness, Mammelzen, Germany) for Vickers hardness testing with a load of 0.049 N. In order to determine differences in the alteration of the transformation temperatures in the weld seam due to the joining process with and without oscillating-beam movement, the system Flash DSC 2 (Mettler Toledo, Gießen, Germany) was used for chip calorimetry. Samples with a weight of about 0.02 mg were taken from the weld seams of the samples with linear laser beam movement and with oscillation with $A = 100 \mu\text{m}$ and $f = 300 \text{ Hz}$ and from the parent material. The samples were heated and cooled in a nitrogen atmosphere between -80 and $180 \text{ }^\circ\text{C}$, and the heat flows were recorded.

3. Results

Figure 2 shows the top and bottom views of the weld seams produced at different values for A and f . The above-mentioned parameters found to be optimal [30] were used as the basis for the systematic variation of A and f ($A = 100 \mu\text{m}$ when f was varied and $f = 300 \text{ Hz}$ when A was varied). All weld seams were fully penetrated and exhibited an even weld seam contour. The traces of the oscillation movement of the laser were differently pronounced on the weld seam surface structure. Figure 2 also shows that the surfaces of the OW samples welded with oscillation were more even overall than those of the LW samples welded with linear laser movement. On some of the samples, dark discolorations were visible along the welds, indicating possible oxidation processes.

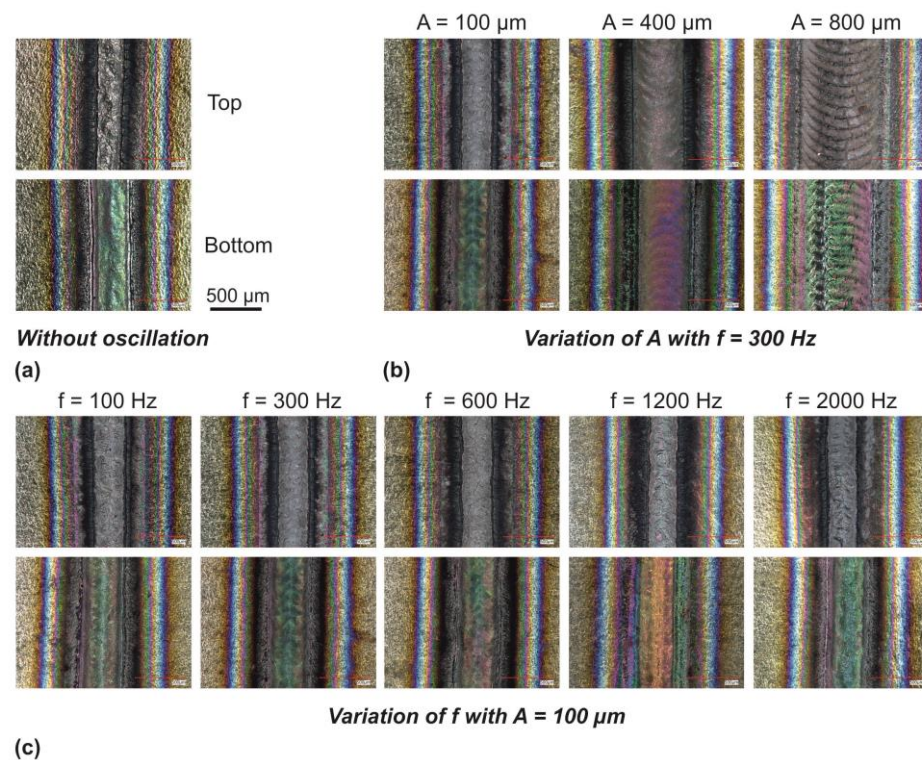


Figure 2. Digital microscopy of the welding seams in top and bottom view (all welds: $P = 40 \text{ W}$, $v = 24 \text{ mm/s}$): (a) welded without oscillation (LW), (b) OW with $f = 300 \text{ Hz}$ and different values of A ; (c) OW with $A = 100 \mu\text{m}$ and different values of f .

All examined welds (OW and LW) had a rectangular weld profile in cross-section, as depicted in Figure 3 by selected examples of LW (Figure 3a-1–a-4) and OW specimens (Figure 3b-1–d-2). The obtained rectangular profile of the welds is typical for laser-welded thin foils and results from high P and a low v values [24]. Likewise, for all samples, the accelerated cooling at the border of the FZ resulted there in a horizontal growth of epitaxial, columnar grains, while vertical grain growth with larger grain sizes was observed in the center of the FZ resulting from cooling through the top and bottom of the weld (Figure 3a-1,b-1,c-1,d-1). The exact extent of the HAZ adjacent to the FZ could only be determined imprecisely for all samples examined, which can be attributed to the annealed initial state of the samples, since the heat treatment had already caused corresponding microstructural transformations [9]. In the FZ of the samples, a certain number of dark and arborescent crystals within the grains and at their boundaries were observed (e.g., Figure 3a-3) that could be attributed to an unanticipated carbon contamination of the parent material, from which titanium carbides were formed [30].

To investigate the influence of the oscillation parameters A and f on the width of the fusion zone, the mean value of the FZ was determined from measurements for the individual samples and plotted against the varied parameter. Figure 4 represents the corresponding results together with the calculated width covered by the laser beam oscillation. The focus diameter was taken into account here and forms the width of the area covered by the laser beam for LW with $A = f = 0$.

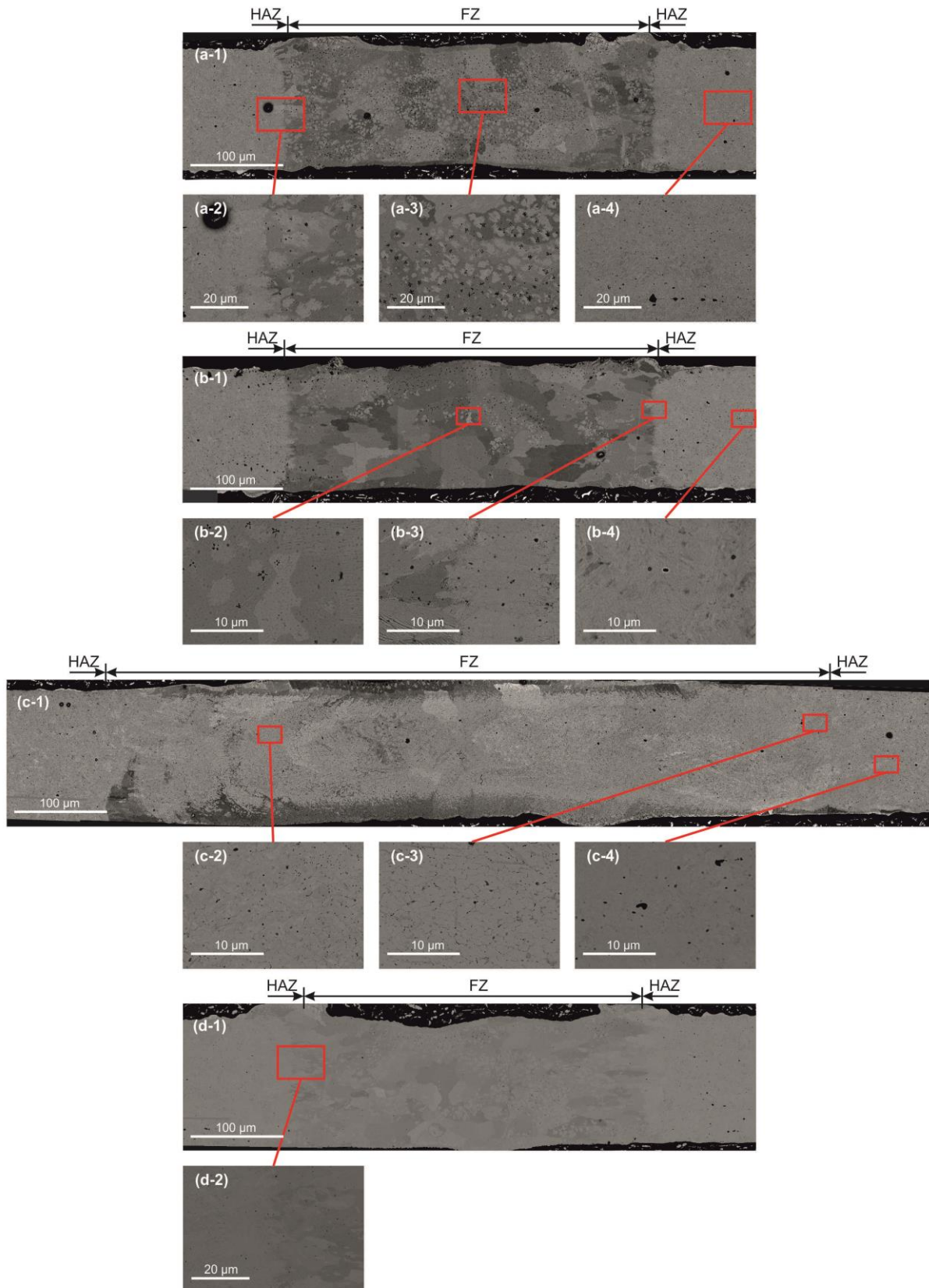


Figure 3. SEM images of microstructure of laser-welded samples (all welds: $P = 40\text{ W}$, $v = 24\text{ mm/s}$): (a-1) LW weld cross-section; (a-2) transition zone; (a-3) FZ; (a-4) parent material; (b-1) OW weld cross-section, $A = 100\ \mu\text{m}$, $f = 300\text{ Hz}$; (b-2) FZ; (b-3) transition zone; (b-4) parent material; (c-1) OW weld cross-section, $A = 800\ \mu\text{m}$, $f = 300\text{ Hz}$; (c-2) FZ; (c-3) transition zone; (c-4) parent material; (d-1) OW weld cross-section, $A = 100\ \mu\text{m}$, $f = 1200\text{ Hz}$; (d-2) transition zone.

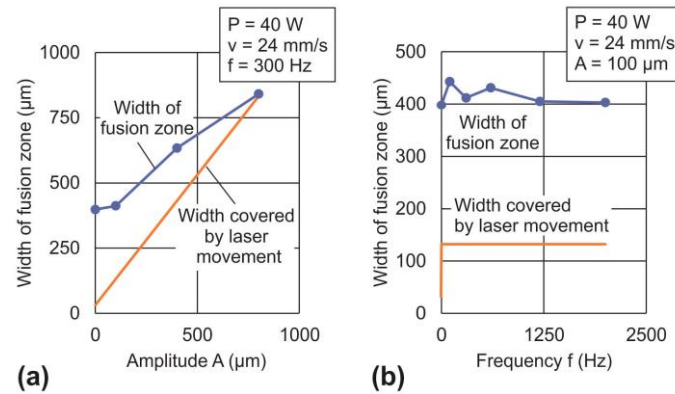


Figure 4. Influence of A and f on the fusion zone width (all welds: $P = 40$ W, $v = 24$ mm/s): (a) for variation of A with $f = 300$ Hz; (b) for variation of f with $A = 100$ µm.

Figure 4a shows that for small values of A , the width of FZ was significantly larger than the width covered by the laser beam. For LW, with $A = 0$, this difference was slightly more than an order of magnitude. As A increased, the width of FZ converged to the area covered by the oscillating laser beam, and in the present case, they matched at an amplitude of about 800 µm. Figure 4b indicates that the frequency f had a significantly smaller effect on the width of FZ in the parameter range examined. With increasing f , the width of FZ became slightly smaller and, at about 2000 Hz, reached the size of FZ without oscillation.

Figure 5 shows examples of the measured hardness along the welded cross-sections of the examined workpieces and the distribution of the selected measuring points for an LW sample (Figure 5a). For the welds without oscillation (LW), an increase in hardness in the FZ compared to the parent material was observed (Figure 5b). With an oscillating laser beam with increasing values of A above 400 µm, however, decreasing hardness values in the FZ were obtained (Figure 5e), which were below those of the parent material. In contrast, an increasing frequency f in the range from 100 to 2000 Hz revealed, with slight reductions in the hardness values, no major significant influence (Figure 5c,f,g).

The microstructure of welds evaluated via EBSD for the LW and OW samples at $A = 100$ µm and different values for f between 100 and 2000 Hz (Figure 6) showed the characteristic configuration of the microstructure of the welds, as previously described for Figure 3. It was found that the analyzed structures of the LW and OW samples exhibited no conspicuous inhomogeneities and were without sub-grains or exceptional grain boundaries. Figure 7 illustrates this by an example of a section of the transition area from the FZ to the HAZ of a sample welded with $A = 100$ µm and $f = 2000$ Hz.

It should be noted that the samples with varied amplitude A (400 and 800 µm) could not be evaluated within the frame of the present work with the available methods, since the EBSD analyses of these samples were associated with a Confidence Index that was too low, and thus, no reliable evaluation of the Kikichi pattern was possible. Improved results may be achieved by using SEM techniques with higher resolution, transmission electron microscopy (TEM) or improved data processing in EBSD, e.g., [50,51]. Furthermore, it is worth mentioning that synchrotron X-ray radiation has also been used to analyze laser-welded Ni-Ti materials [9]. Regarding an improved data processing, the authors are currently investigating the use of artificial intelligence to obtain enhanced analysis results and to examine the causes of the correlations found and described in this paper in more detail, using further characterization methods, for example, as described in [52] for a laser-treated Ti-alloy.

More precise microstructural information was obtained from the evaluation of the ranges of grain area size based on these observations, illustrated in Figure 8. According to

this, the application of laser beam oscillation resulted in grain refinement of up to 66%. While the mean grain area size of the LW samples was about $1030 \mu\text{m}^2$, it was between $347 \mu\text{m}^2$ ($f=1200 \text{ Hz}$) and $903 \mu\text{m}^2$ ($f=300 \text{ Hz}$) for the OW samples. Overall, an alternating trend in the influence of frequency on grain size was observed, with grain refinement between the frequencies 300 and 1200 Hz and an increase at $f=2000 \text{ Hz}$ to an average grain area size of $526 \mu\text{m}^2$.

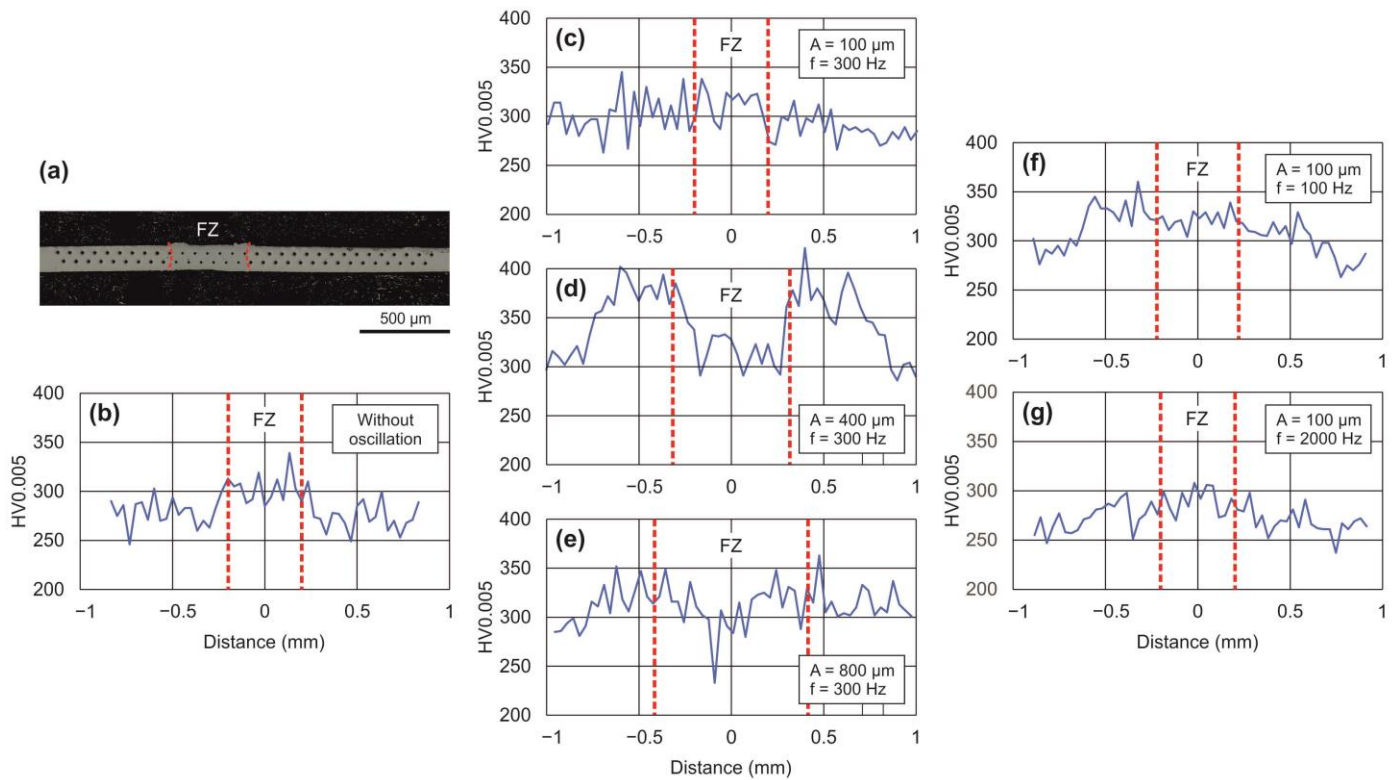


Figure 5. Results of microhardness measurements (all welds: $P = 40 \text{ W}$, $v = 24 \text{ mm/s}$): (a) measured locations (LW sample); (b) hardness distribution without oscillation of laser beam (LW); (c) hardness distribution for $A = 100 \mu\text{m}$, $f = 300 \text{ Hz}$ (OW); (d) $A = 400 \mu\text{m}$, $f = 300 \text{ Hz}$; (e) $A = 800 \mu\text{m}$, $f = 300 \text{ Hz}$; (f) $A = 100 \mu\text{m}$, $f = 100 \text{ Hz}$; (g) $A = 100 \mu\text{m}$, $f = 2000 \text{ Hz}$.

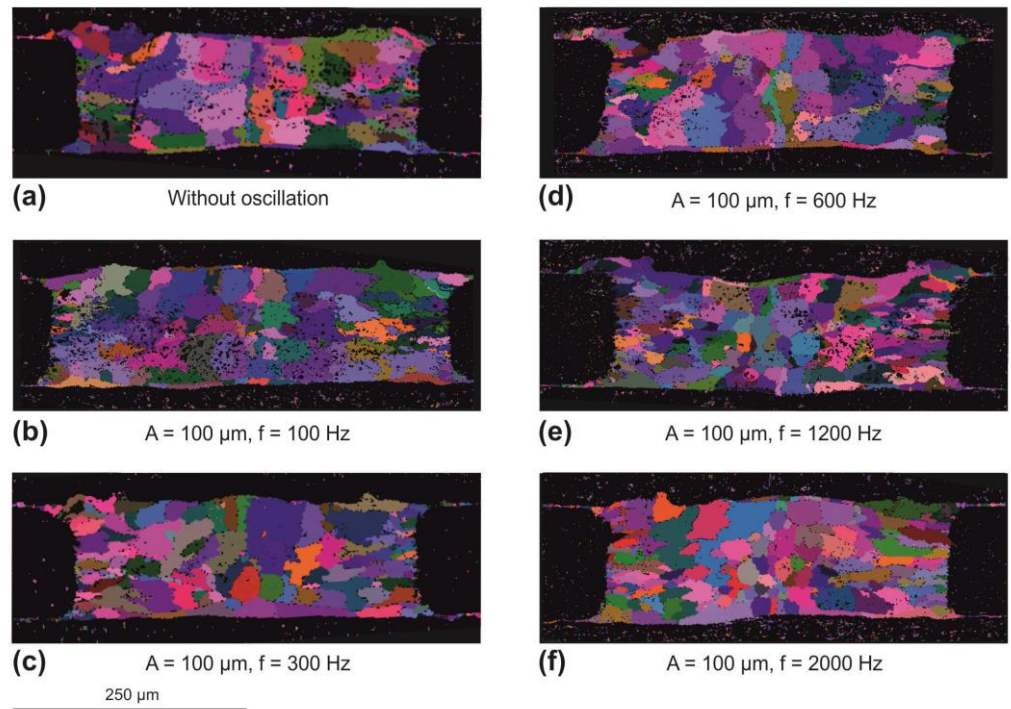


Figure 6. EBSD analysis of the microstructure in the FZ cross-sectional view (Euler maps, all welds: $P = 40\text{ W}$, $v = 24\text{ mm/s}$ and OW welds with $A = 100\text{ }\mu\text{m}$): (a) without oscillation (LW); (b) OW with $f = 100\text{ Hz}$; (c) $f = 300\text{ Hz}$; (d) $f = 600\text{ Hz}$; (e) $f = 1200\text{ Hz}$; (f) $f = 2000\text{ Hz}$.

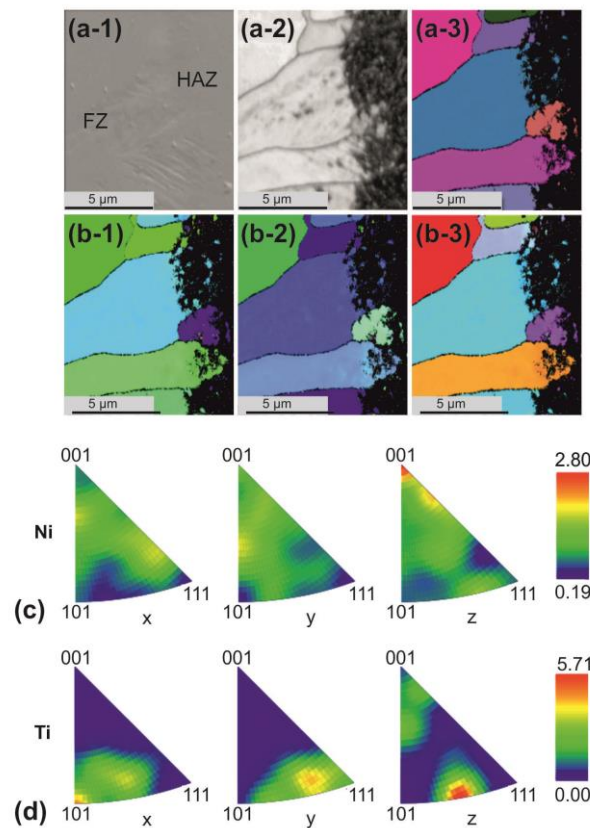


Figure 7. EBSD analysis of the transition zone from FZ to HAZ for an OW weld fabricated with $P = 40\text{ W}$, $v = 24\text{ mm/s}$, $A = 100\text{ }\mu\text{m}$ and $f = 2000\text{ Hz}$: (a-1) SEM image of the analyzed area; (a-2) band contrast image; (a-3) Euler map; (b-1) inverse pole figure map IPF-X; (b-2) IPF-Y; (b-3) IPF-Z; map (c) IPFs of Ni; (d) IPFs of Ti.

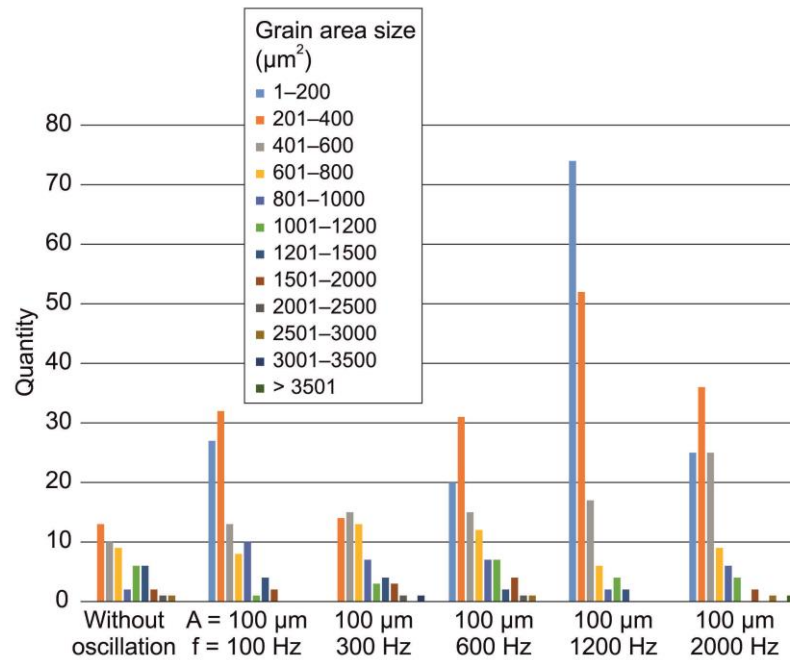


Figure 8. Software-supported analysis of grain area sizes in the FZ based on SEM results for the samples LW and OW with $A = 100 \mu\text{m}$ and different f (all welds: $P = 40 \text{ W}$, $v = 24 \text{ mm/s}$).

An analysis of the material composition was carried out for the FZ of an OW sample with $A = 100 \mu\text{m}$ and $f = 1200 \mu\text{m}$ using EDX (Figure 9). According to these results, this sample showed the chemical material composition of the parent material in the FZ, but with localized Ni/Ti/C/O-rich phases in the peripheral area and local Ti-C compounds (Figure 9). The carbon, which is usually not part of the investigated shape memory alloy, can be attributed to the impurities described above. The presence of oxygen is attributed to oxidation processes on the weld surface during the joining process, which occurred despite the use of inert shielding gas. It is suspected that turbulences caused by the crossjet used to keep the lens system clean carried oxygen into the shielding gas bath. This was also indicated by the oxidation layer on the weld surface, as determined by EDX (Figure 9). It should be noted that due to the small dimensions of the weld, the surface-to-volume ratio is much greater than for welds in the conventional macro range. This favors the influence of surface-related processes [53], such as diffusion. However, to substantiate the existence of such size effects, more investigations are still needed to examine specific comparisons of conventional and downscaled dimensions of laser-welded seams and the specific oxygen content.

Overall, local separations of the alloying elements were observed in the center of the FZ of the LW and OW specimens, as shown in Figure 10 by the example of a specimen welded with $A = 100 \mu\text{m}$ and $f = 2000 \text{ Hz}$. On the basis of the analyzed spectra, phases with a higher Ti content could be identified (the light-gray areas in Figure 10) and structures with a high proportion of Ti and C were determined (the black branched areas in Figure 10).

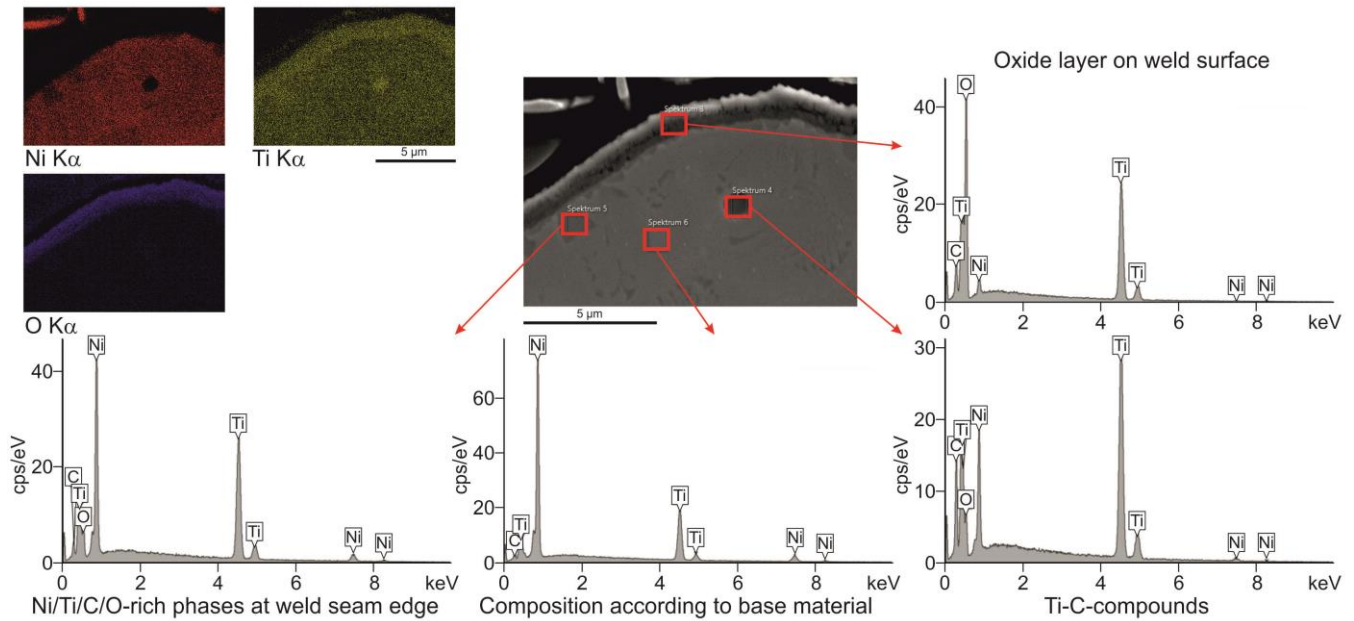


Figure 9. EDX analysis of the material composition in the FZ on the upper outer edge of an OW sample produced with $A = 100 \mu\text{m}$, $f = 1200 \text{ Hz}$, $P = 40 \text{ W}$ and $v = 24 \text{ mm/s}$.

The chip calorimetry method was used to investigate changes in the transformation temperatures caused by the welding process. For this purpose, material samples were taken from the fusion zones of an OW specimen welded with the oscillation parameters $A = 100 \mu\text{m}$ and $f = 300 \text{ Hz}$ and from a LW specimen. The heating and cooling curves obtained for these samples are compiled in Figure 11 together with the curves of the parent material, which were also recorded.

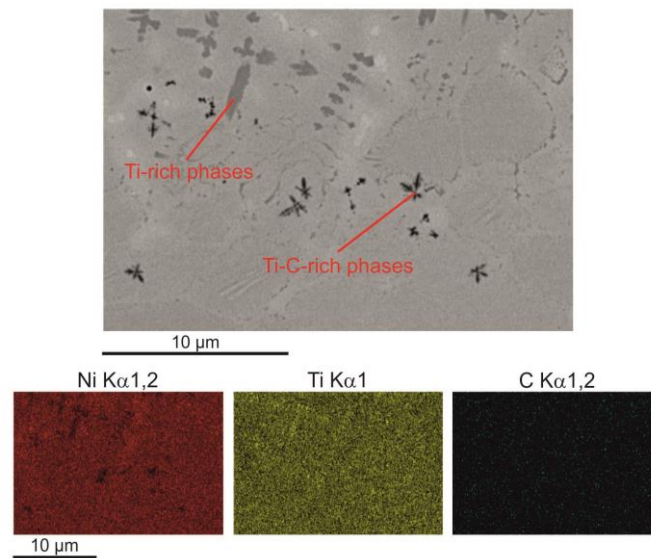


Figure 10. EDX analysis of the material composition in the FZ center of an OW sample produced with $A = 100 \mu\text{m}$, $f = 2000 \text{ Hz}$, $P = 40 \text{ W}$, and $v = 24 \text{ mm/s}$.

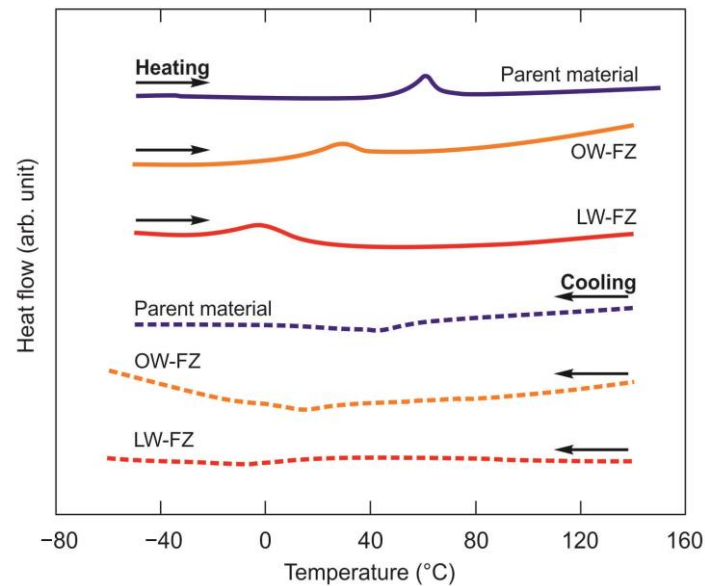


Figure 11. Chip calorimetry results (all welds: $P = 40$ W, $v = 24$ mm/s); OW-FZ: sample from FZ of specimen welded with $A = 100$ μm and $f = 300$ Hz; LW-FZ: sample from FZ of specimen welded without oscillation.

The behavior of all samples showed the characteristic differential scanning calorimetry curves of an annealed Ni-Ti alloy with exothermic and endothermic peaks, indicating the microstructural transformations between B2 and B19' phases. The presence of R-phase transformations, which would have resulted in several separated peaks, was not readily apparent for the analyzed samples. The comparison of the transformation curves of the parent material and the FZs of the OW and LW samples indicated that the transformation temperatures of the welds were below those of the parent material and that those of the LW samples decreased more than those of the OW specimens. However, it should be noted that the measurements were carried out without a melting standard on the reference side of the heat flow sensor, which means that the sample size could have affected the measured temperatures. Further investigations are planned in this context.

4. Discussion

The results presented above show that the superimposition of an oscillating laser beam movement for welding of the investigated Ni-Ti alloy influenced the weld seam property with regard to the formation of the FZ, the mechanical–technological properties, the microstructure, and the transformation behavior.

Regarding the influence of A and f on the width of the FZ, it was found that FZ becomes wider with increasing amplitude A (Figure 4), but not in the same proportion as the width covered by the moving laser increases. This is due to the fact that with increasing amplitude of the laser beam, the energy density along its path decreases because the energy is distributed over a longer path. This means that lower temperature gradients can be expected in the weld compared to welding without oscillation, which benefits the formation of a more favorable solidification microstructure [31]. In the present case, the width of the FZ and the width covered by the laser coincided at about $A = 800$ μm . However, in [30], the authors determined that the favorable strength values of the weld can be expected with $A = 300$ μm . This suggests that further effects, besides the adjusting of energy density and temperature gradients, play a role in the selection of an optimal value for A , where high strengths are the main focus for the Ni-Ti alloy investigated here. Consequently, further investigations are still needed, also, for example, analyzing possible

effects resulting from solution strengthening. Also, there may be a correlation here between the hardness of the weld, which decreased with increasing A , below the values of the parent material (Figure 5) and the tensile strength. The finding that the FZ width reduced when f increased is consistent with studies on stainless steel [48] and was also related to the change in energy density.

The determined higher hardness of the weld seam in comparison to the parent material for LW samples and OW samples that were welded with A up to 400 μm (Figure 5) appears exceptional but can be attributed to findings in [19], where it was determined on LW samples made of a Ni-Ti alloy that, depending on the thermal–mechanical history of the parent material, the hardness values can both decrease and increase. The material used for the present investigations was supplied by the manufacturer as annealed and was not treated further. However, it is important to note that the influence of the amplitude A on the hardness of the weld was greater than the influence of the frequency f (Figure 5).

With regard to the influence of f on grain refinement, the results of this study are consistent with those for oscillating welding of an invar alloy presented in [46], according to which grain refinement occurred up to a certain limit of f , beyond which no further improvement in the microstructure was visible. In the present work, a continuous decrease in grain size was observed with increasing frequency up to $f = 1200$ Hz (66% decrease compared to welding without oscillation) and also an increase at $f = 2000$ Hz of about 52% compared to the welding at $f = 1200$ Hz (Figure 8). At present, only tentative assumptions can be made regarding the exact cause of the grain size increase above $f = 1200$ Hz: With increasing frequency, the locally introduced energy of the moving laser beam typically decreases and, in principle, with it the energy that can locally contribute to the formation of vortices. This would mean a reduction in the stirring effect with increasing f , which, however, would have to be observed already at frequencies below 1200 Hz with the associated grain coarsening. Since this was not the case, and also the work in [48] showed an increasing flow in the melted material with increasing f , it is assumed that the reason for the observed trend was rather the frequency-dependent effects of heat accumulation described in [46] than a weakening in the stirring effect. However, the exact causes still need to be investigated in more detail, for example, by applying suitable simulation models to study the oscillation-dependent heat development and melt flow [38]. Furthermore, the influence of A requires more detailed investigation.

The advantage of the conducted chip calorimetry measurements was that a very limited area of the FZ could be analyzed without influences from neighboring areas, such as the HAZ or the parent material, affecting the results. It was shown that the measurements can be used to draw conclusions about the transformation temperatures (Figure 11), although further analyses are needed with regard to calibration. In the form of the measurements carried out, these suggested that the welding process caused a decrease in the transformation temperatures, which was mitigated by using laser beam oscillation. Possible causes of the decrease in the transformation temperatures could be attributed, in the present case, to the detected oxygen content (Figure 9) in the FZ [9,20]. The micro-welding of thin Ni-Ti foils investigated here was associated with a significantly higher weld surface-to-volume ratio compared to the welding of conventionally dimensioned Ni-Ti sheets with a thickness of several millimeters. The consequence of this is that, with thin foils, surface-relevant processes such as oxygen absorption can have a significantly stronger effect on material alterations in the FZ compared to conventional welding dimensions. Likewise, local separation of alloying elements was detected in the FZ (Figure 10), which inevitably led to a local change in the Ni-Ti composition and thus to altered properties with regard to the shape memory effect and superelasticity. Therefore, further research is planned to determine the effect of the oscillation parameters on the uniformity of the distribution of alloying elements.

5. Conclusions

The present study systematically investigated the influence of amplitude and frequency of a circularly oscillating laser beam movement for joining thin foils with a thickness of 125 μm made of a Ni-Ti alloy. According to the results, an increasing amplitude led to decreasing hardness values of the weld seam, while the influence of the frequency was smaller. By increasing the frequency, grain refinement could be achieved up to a certain value of the frequency. The analyses with chip calorimetry suggested a reduction in the transformation temperatures in the fusion zone due to the welding process, which was mitigated by the use of superimposed laser beam oscillation.

Author Contributions: Conceptualization, methodology, supervision, review—editing, D.K.-K.; formal analysis, investigations, S.W.; conceptualization, methodology, supervision, writing—original draft preparation, C.H. All authors have read and agreed to the published version of the manuscript.

Funding: This research received no external funding.

Data Availability Statement: All data supporting the results of the described research study are available in the publication and no associated data were generated.

Acknowledgments: The authors thank Jonas Kotscha for welding the samples and Jürgen Keden from Metler Toledo for performing the chip calorimetry measurements.

Conflicts of Interest: The authors declare no conflicts of interest.

References

1. Costanza, G.; Tata, M.E. Shape Memory Alloys for Aerospace, Recent Developments, and New Applications: A Short Review. *Materials* **2020**, *13*, 1856. <https://doi.org/10.3390/ma13081856>.
2. Stachiv, I.; Alarcon, E.; Lamac, M. Shape Memory Alloys and Polymers for MEMS/NEMS Applications: Review on Recent Findings and Challenges in Design, Preparation, and Characterization. *Metals* **2021**, *11*, 415. <https://doi.org/10.3390/met11030415>.
3. McCracken, J.M.; Donovan, B.R.; White, T.J. Materials as Machines. *Adv. Mater.* **2020**, *32*, 1906564. <https://doi.org/10.1002/adma.201906564>.
4. Holman, H.; Kavarana, M.N.; Rajab, T.K. Smart materials in cardiovascular implants: Shape memory alloys and shape memory polymers. *Artif. Organs* **2021**, *45*, 454–463. <https://doi.org/10.1111/aor.13851>.
5. Datta, S.; Raza, M.S.; Das, A.K.; Saha, P.; Pratihari, D.K. Experimental investigations and parametric optimization of laser beam welding of NiTiInol sheets by metaheuristic techniques and desirability function analysis. *Opt. Laser Technol.* **2020**, *124*, 105982. <https://doi.org/10.1016/j.optlastec.2019.105982>.
6. Mehrpouya, M.; Gisario, A.; Elahinia, M. Laser welding of NiTi shape memory alloy: A review. *J. Manuf. Process.* **2018**, *31*, 162–186. <https://doi.org/10.1016/j.jmapro.2017.11.011>.
7. Parimanik, S.R.; Mahapatra, T.R.; Mishra, D. A Systematic Literature Review on Laser Welding of NiTi SMA. *Lasers Manuf. Mater. Process.* **2023**, *10*, 77–117. <https://doi.org/10.1007/s40516-022-00200-7>.
8. Otsuka, K.; Ren, X. Physical metallurgy of Ti–Ni-based shape memory alloys. *Prog. Mater. Sci.* **2005**, *50*, 511–678. <https://doi.org/10.1016/j.pmatsci.2004.10.001>.
9. Oliveira, J.P.; Miranda, R.M.; Braz Fernandes, F.M. Welding and Joining of NiTi Shape Memory Alloys: A Review. *Prog. Mater. Sci.* **2017**, *88*, 412–466. <https://doi.org/10.1016/j.pmatsci.2017.04.008>.
10. Kumar, P.K.; Lagoudas, D.C. Introduction to Shape Memory Alloys. In *Shape Memory Alloys: Modeling and Engineering Applications*. Lagoudas, D.C., Ed.; Springer: Boston MA, USA, 2008; Volume 1, pp. 1–119. https://doi.org/10.1007/978-0-387-47685-8_1.
11. Dolce, M.; Cardone, D. Mechanical behaviour of shape memory alloys for seismic applications 2. Austenite NiTi wires subjected to tension. *Int. J. Mech. Sci.* **2001**, *43*, 2657–2677. [https://doi.org/10.1016/S0020-7403\(01\)00050-9](https://doi.org/10.1016/S0020-7403(01)00050-9).
12. Mehta, K.; Gupta, K. *Fabrication and Processing of Shape Memory Alloys*; Springer: Cham, Switzerland, 2019. <https://doi.org/10.1007/978-3-319-99307-2>.
13. Ternik, P.; Rudolf, R. Numerical Analysis of Continuous Casting of NiTi Shape Memory Alloy. *Int. J. Simul. Model.* **2016**, *15*, 522–531.

14. Parvizi, S.; Hashemi, S.M.; Asgarinia, F.; Nematollahib, M.; Mohammad, E. Effective parameters on the final properties of NiTi-based alloys manufactured by powder metallurgy methods: A review. *Prog. Mater. Sci.* **2021**, *117*, 100739. <https://doi.org/10.1016/j.pmatsci.2020.100739>.
15. Gerstein, G.; Kahra, C.; Golovko, O.; Schäfke, F.; Klose, C.; Herbst, S.; Nürnberger, F.; Maier, H.J. Hot forming of shape memory alloys in steel shells: Formability, interface, bonding quality. *Prod. Eng.* **2021**, *15*, 271–283. <https://doi.org/10.1007/s11740-021-01024-8>.
16. Shizuka, H.; Sakai, K.; Yang, H.; Sonoda, K.; Nagare, T.; Kurebayashi, Y.; Hayakawa, K. Difficult Cutting Property of NiTi Alloy and Its Mechanism. *J. Manuf. Mater. Process.* **2020**, *4*, 124. <https://doi.org/10.3390/jmmp4040124>.
17. Li, B.; Wang, L.; Wang, B.; Li, D.; Oliveira, J.P.; Cui, R.; Yu, J.; Luo, L.; Chen, R.; Su, Y.; et al. Tuning the microstructure, martensitic transformation and superelastic properties of EBF³-fabricated NiTi shape memory alloy using interlayer remelting. *Mater. Des.* **2022**, *220*, 110886. <https://doi.org/10.1016/j.matdes.2022.110886>.
18. Timercan, A.; Campion, D.; Terriault, P.; Brailovski, V. Laser Powder Bed Fusion of Superelastic Ti-Ni Lattice Structures: Process Design and Testing. *J. Manuf. Mater. Process.* **2024**, *8*, 176. <https://doi.org/10.3390/jmmp8040176>.
19. Tuissi, A.; Besseghini, S.; Ranucci, T.; Squatrito, F.; Pozzi, M. Effect of Nd-YAG laser welding on the functional properties of the Ni-49.6at.%Ti. *Mater. Sci. Eng. A* **1999**, *273–275*, 813–817. [https://doi.org/10.1016/S0921-5093\(99\)00422-0](https://doi.org/10.1016/S0921-5093(99)00422-0).
20. Hsu, Y.T.; Wang, Y.R.; Wu, S.K.; Chen, C. Effect of CO₂ laser welding on the shape-memory and corrosion characteristics of TiNi alloys. *Metall. Mater. Trans. A* **2001**, *32*, 569–576. <https://doi.org/10.1007/s11661-001-0073-2>.
21. Vertegaal, C.J.C.; Bentum, M.J.; Pourshaghghi, H.R. Using Shape Memory Alloy for CubeSat Antenna. In Proceedings of the 15th European Conference on Antennas and Propagation (EuCAP), Düsseldorf, Germany, 22–26 March 2021. <https://doi.org/10.23919/EuCAP51087.2021.9411188>.
22. Garcés-Schröder, M.; Zimmermann, T.; Siemers, C.; Leester-Schädel, M.; Böhl, M.; Dietzel, A. Shape Memory Alloy Actuators for Silicon Microgrippers. *J. Microelectromech. Syst.* **2019**, *28*, 869–881. <https://doi.org/10.1109/JMEMS.2019.2936288>.
23. Khan, M.I.; Panda, S.K.; Zhou, Y. Effects of Welding Parameters on the Mechanical Performance of Laser Welded Nitinol. *Mater. Trans.* **2008**, *49*, 2702–2708. <https://doi.org/10.2320/matertrans.MRA2008243>.
24. Chan, C.W.; Man, H.C.; Yue, T.M. Effects of Process Parameters upon the Shape Memory and Pseudo-Elastic Behaviors of Laser-Welded NiTi Thin Foil. *Metall. Mater. Trans. A* **2011**, *42*, 2264–2270. <https://doi.org/10.1007/s11661-011-0623-1>.
25. Gong, W.; Chen, Y.; Ke, L. Microstructure and properties of laser micro welded joint of TiNi shape memory alloy. *Trans. Non-ferrous Met. Soc. China* **2011**, *21*, 2044–2048. [https://doi.org/10.1016/S1003-6326\(11\)60970-9](https://doi.org/10.1016/S1003-6326(11)60970-9).
26. Quintino, L.; Miranda, R.M. Welding Shape Memory Alloys with NdYAG lasers. *Soldag. Insp. São Paulo* **2012**, *17*, 210–217. Available online: <https://www.scielo.br/j/si/a/x3VqNWbZVB7PvchQShwQWxM/?format=pdf&lang=en> (accessed on 8 December 2024).
27. Oliveira, J.P.; Braz Fernandes, F.M.; Miranda, R.M.; Shell, N. On the Mechanisms for Martensite Formation in YAG Laser Welded Austenitic NiTi. *Shap. Mem. Superelasticity* **2016**, *2*, 114–120. <https://doi.org/10.1007/s40830-016-0058-z>.
28. Kannan, T.D.B.; Ramesh, T.; Sathiya, P. Application of Artificial Neural Network Modelling for Optimization of Yb: YAG Laser Welding of Nitinol. *Trans. Indian Inst. Met.* **2017**, *70*, 1763–1771. <https://doi.org/10.1007/s12666-016-0973-x>.
29. Datta, S.; Raza, M.S.; Saha, P.; Pratihar, D.K. Effects of process parameters on the quality aspects of weld-bead in laser welding of NiTi sheets. *Mater. Manuf. Process.* **2019**, *34*, 648–659. <https://doi.org/10.1080/10426914.2019.1566608>.
30. Katrakova-Krüger, D.; Pegoraro, L.; Salmaso, L.; Hartl, C.; Schulz, I.; Weichert, S.; Steffen, R. Laser Welding of Nitinol Thin Foils: Mechanical Properties and Microstructure Depending on Process Parameters. *Metall. Mater. Trans. A* **2023**, *54*, 998–1009. <https://doi.org/10.1007/s11661-022-06954-1>.
31. Norouzian, M.; Elahi, M.A.; Plapper, P. A review: Suppression of the solidification cracks in the laser welding process by controlling the grain structure and chemical compositions. *J. Adv. Join. Process.* **2023**, *7*, 100139. <https://doi.org/10.1016/j.jajp.2023.100139>.
32. Wang, Z.; Gao, M. Numerical simulations of oscillating laser welding: A review. *J. Manuf. Process.* **2024**, *119*, 744–757. <https://doi.org/10.1016/j.jmapro.2024.04.001>.
33. Hensel, J.; Köhler, M.; Uhlenberg, L.; Dinize Castro, J.; Dilger, K.; Faß, M.; Baumgartner, J. Laser welding of 16MnCr5 butt welds with gap: Resulting weld quality and fatigue strength assessment. *Weld. World* **2022**, *66*, 1867–1881. <https://doi.org/10.1007/s40194-022-01306-4>.
34. Das, A.; Masters, I.; Williams, D. Understanding novel gap-bridged remote laser welded (RLW) joints for automotive high-rate and temperature applications. *Int. J. Mech. Sci.* **2021**, *190*, 106043. <https://doi.org/10.1016/j.jimecs.2020.106043>.

35. Hu, C.; Zhu, Z.; Wang, C. Optimization of beam oscillation on macro/micro formation and mechanical property in low-expansion superalloy laser-welded joint. *J. Mater. Res. Technol.* **2022**, *17*, 1259–1273. <https://doi.org/10.1016/j.jmrt.2022.01.108>.
36. Hao, Y.; Li, L.; Sun, Y.; Shao, C.; Lu, F. Dynamic behavior of keyhole and molten pool under different oscillation paths for galvanized steel laser welding. *Int. J. Heat Mass Transf.* **2022**, *192*, 122947. <https://doi.org/10.1016/j.ijheatmasstransfer.2022.122947>.
37. Chen, C.; Zhou, H.; Wang, C.; Liu, L.; Zhang, Y.; Zhang, K. Laser welding of ultra-high strength steel with different oscillating modes. *J. Manuf. Process.* **2021**, *68A*, 761–769. <https://doi.org/10.1016/j.jmapro.2021.06.004>.
38. Ke, W.; Bu, X.; Oliveira, J.P.; Xu, W.G.; Wang, Z.; Zeng, Z. Modeling and numerical study of keyhole-induced porosity formation in laser beam oscillating welding of 5A06 aluminum alloy. *Opt. Laser Technol.* **2021**, *133*, 106540. <https://doi.org/10.1016/j.optlastec.2020.106540>.
39. Zhou, X.; Zhao, H.; Liu, F.; Yang, B.; Xu, B.; Chen, B.; Tang, C. Effects of beam oscillation modes on microstructure and mechanical properties of laser welded 2060 Al-Li alloy joints. *Opt. Laser Technol.* **2021**, *144*, 107389. <https://doi.org/10.1016/j.optlastec.2021.107389>.
40. Tan, Z.; Pang, B.; Oliveira, J.P.; Chen, L.; Bu, X.; Wang, Z.; Cong, B.; Zeng, Z. Effect of S-curve laser power for power distribution control on laser oscillating welding of 5A06 aluminum alloy. *Opt. Laser Technol.* **2022**, *149*, 107909. <https://doi.org/10.1016/j.optlastec.2022.107909>.
41. Lei, Z.; Chen, Y.; Zhou, H.; Wang, X.; Liu, J.; Xia, P. Melt flow and grain refining in laser oscillating welding of β -21S titanium alloy. *Opt. Laser Technol.* **2022**, *145*, 107496. <https://doi.org/10.1016/j.optlastec.2021.107496>.
42. Zhang, C.; Yu, Y.; Chen, C.; Zeng, X.; Gao, M. Suppressing porosity of a laser keyhole welded Al-6Mg alloy via beam oscillation. *J. Mater. Process. Technol.* **2020**, *278*, 116382. <https://doi.org/10.1016/j.jmatprotec.2019.116382>.
43. Zhao, X.; Chen, J.; Lei, Z.; Zhang, W.; Hui Chen, H. A study on the flow behavior and bubble evolution of circular oscillating laser welding of SUS301L-HT stainless steel. *Int. J. Heat Mass Transf.* **2023**, *202*, 123726. <https://doi.org/10.1016/j.ijheatmasstransfer.2022.123726>.
44. Liu, M.; Shao, C.; Zheng, Z.; Lu, F. The effect of laser oscillation welding on porosity suppression for medium-thick Al alloy with high Mg content. *Opt. Laser Technol.* **2024**, *175*, 110795. <https://doi.org/10.1016/j.optlastec.2024.110795>.
45. Wang, L.; Gao, M.; Hao, Z.: A pathway to mitigate macrosegregation of laser-arc hybrid Al-Si welds through beam oscillation. *Int. J. Heat Mass Transf.* **2020**, *151*, 119467. <https://doi.org/10.1016/j.ijheatmasstransfer.2020.119467>.
46. Zhao, J.; Wang, J.; Kang, X.; Wang, X.; Zhan, X. Effect of beam oscillation and oscillating frequency induced heat accumulation on microstructure and mechanical property in laser welding of Invar alloy. *Opt. Laser Technol.* **2023**, *158*, 108831. <https://doi.org/10.1016/j.optlastec.2022.108831>.
47. Cai, J.; Wei, Y.; Ouyang, Z.; Liu, X.; Jin, H.; Chen, J. Investigation on clockwise circular oscillating laser welding for the 5A06-H112 aluminum alloy: Energy distribution, seam appearance, microstructure, and mechanical properties. *Opt. Laser Technol.* **2024**, *176*, 111026. <https://doi.org/10.1016/j.optlastec.2024.111026>.
48. Dong, B.; Li, Z.; Chen, B.; He, X. Effect of oscillation parameters on weld surface morphology during laser beam oscillation welding of stainless steel. *Int. J. Therm. Sci.* **2025**, *207*, 109339. <https://doi.org/10.1016/j.ijthermalsci.2024.109339>.
49. DIN EN ISO 6507-1:2023, Metallic materials - Vickers hardness test - Part 1: Test method. Beuth-Verlag: Berlin, Germany, 2023.
50. De Haan, K.; Ballard, Z.S.; Rivenson, Y.; Wu, Y.; Ozcan, A. Resolution enhancement in scanning electron microscopy using deep learning. *Sci. Rep.* **2019**, *9*, 12050. <https://doi.org/10.1038/s41598-019-48444-2>.
51. Andrews, C.E.; Strantza, M.; Calta, N.P.; Matthews, M.J.; Taheri, M.L. A Denoising Autoencoder for Improved Kikuchi Pattern Quality and Indexing in Electron Backscatter Diffraction. *Ultramicroscopy* **2023**, *253*, 113810. <https://doi.org/10.1016/j.ultramic.2023.113810>.
52. Ouyang, W.; Zhang, L.; Wu, H.; Wu, D.; Zhang, S.; Qin, X.; Jiang, S.; Li, S.; Zhang, W.; Sheng, L. Optimized mechanical properties of the hot forged Ti-6Al-4V alloy by regulating multiscale microstructure via laser shock peening. *Int. J. Mach. Tools Manuf.* **2024**, *201*, 104192. <https://doi.org/10.1016/j.ijmachtools.2024.104192>.
53. Vollertsen, F.; Schulze Niehoff, H.; Hu, Z. State of the art in micro forming. *Int. J. Mach. Tools Manuf.* **2006**, *46*, 1172–1179. <https://doi.org/10.1016/j.ijmachtools.2006.01.033>.

Disclaimer/Publisher's Note: The statements, opinions and data contained in all publications are solely those of the individual author(s) and contributor(s) and not of MDPI and/or the editor(s). MDPI and/or the editor(s) disclaim responsibility for any injury to people or property resulting from any ideas, methods, instructions or products referred to in the content.